

## Article

# Development of Hexagonal Pyramid-Shaped Flexible Actuator with Anisotropic Stiffness for Upper-Limb Rehabilitation Device

So Shimooka <sup>1,\*</sup> , Hiroki Himuro <sup>2</sup> and Akio Gofuku <sup>2</sup>

<sup>1</sup> Faculty of Environmental, Life, Natural Science and Technology, Okayama University, 3-1-1 Tsushima-Naka, Kita-ku, Okayama 700-8530, Japan

<sup>2</sup> Faculty of Interdisciplinary Science and Engineering in Health Systems, Okayama University, 3-1-1 Tsushima-Naka, Kita-ku, Okayama 700-8530, Japan; himuro0h0mif@s.okayama-u.ac.jp (H.H.); gofuku-a@okayama-u.ac.jp (A.G.)

\* Correspondence: shimooka@okayama-u.ac.jp

**Abstract:** Rehabilitation devices for passive exercise have been actively researched and developed in accordance with Japan's aging society. A previous study proposed and tested an extension-type flexible pneumatic actuator (EFPA) with reinforced stiffness that could achieve passive exercise in patients. In addition, a rehabilitation device for shoulder joints with an embedded controller and small valves was proposed and tested. Joints such as the shoulder and scapula were subjected to passive exercise utilizing the tested device. However, it is difficult for patients with contractions to perform the same exercise because the reinforced EFPA can buckle. Here, to realize an EFPA with a higher stiffness, a flexible actuator in the shape of a hexagonal pyramid is proposed and tested. The hexagonal pyramid shape of a flexible actuator has a high stiffness in the direction of motion and flexibility in other directions; hereafter, this characteristic is called anisotropic stiffness. The characteristics of the hexagonal pyramid shape of the EFPA are described and compared with those of a previously reinforced EFPA. An analytical model was proposed to predict and design the shape of the hexagonal pyramid EFPA. The validity of the model is also described.

**Keywords:** hexagonal pyramid shape of flexible actuator; anisotropic stiffness; extension-type flexible pneumatic actuator; analytical model of shape



**Citation:** Shimooka, S.; Himuro, H.; Gofuku, A. Development of Hexagonal Pyramid-Shaped Flexible Actuator with Anisotropic Stiffness for Upper-Limb Rehabilitation Device. *Actuators* **2023**, *12*, 424. <https://doi.org/10.3390/act12110424>

Academic Editors: Hongliang Ren and Jiewen Lai

Received: 13 September 2023  
Revised: 9 November 2023  
Accepted: 13 November 2023  
Published: 14 November 2023



**Copyright:** © 2023 by the authors. Licensee MDPI, Basel, Switzerland. This article is an open access article distributed under the terms and conditions of the Creative Commons Attribution (CC BY) license (<https://creativecommons.org/licenses/by/4.0/>).

## 1. Introduction

The number of older adults and the reduction in infant birth rates in Japan have increased. The proportion of older adults aged 65 and over was 29.1% in 2022 [1]. This ratio is expected to be approximately 36% by 2040. This rate is the highest worldwide and is a serious problem in Japan because the physical functions of older adults decline with age. When older adults develop a disuse syndrome and require nursing care, they must recover their physical function as early as possible. Taking account of “Quality of Life” for older adults or patients, they are given a passive exercise by a physical therapist (PT) and an occupational therapist (OT). According to Japanese law, a PT and OT cannot provide rehabilitation for patients for just 30 min per day. However, based on the opinions of on-site PTs and OTs, they recognized that rehabilitation for 30 min is insufficient. They recommend that patients carry out voluntary rehabilitation and exercise at home. Medical reports have proposed the necessity of voluntary rehabilitation to prevent various diseases and disuse syndromes [2]. However, it is difficult for older adults to exercise voluntarily for a long time because of their declining physical function and motivation. Therefore, a rehabilitation device that can safely provide passive exercises is desirable. To address these issues, various wearable and rehabilitation devices that support exercise and nursing care have been actively researched and developed [3–11]. Joints such as the upper limbs and legs were effectively exercised utilizing these devices. However, from reference [3–5], previous rehabilitation devices for the upper limbs do not have flexible

motion and back-drivability, similar to physical and occupational therapists. In addition, users must utilize and attach devices, and the range of motion of the upper limbs is limited. If the device malfunctions, the user may be injured. Therefore, these devices must be adjusted to ensure user safety. Operators such as PTs and OTs must monitor users because they cannot adjust their physical functions. We believe that the burden on PTs and OTs has increased owing to monitoring. Ideally, devices that can adjust a patient's physical function without an operator are required. Patients should release these devices immediately when they are in danger of undergoing rehabilitation. Recently, soft actuators made of polymeric materials such as rubber have been utilized in rehabilitation and wearable devices [12–25]. These soft actuators are lightweight, flexible, highly human-friendly, and safe because of their compliance and softness. Therefore, devices that utilize a soft actuator with a driven fluid-powered system are suitable for rehabilitation and motion assistance [26].

We attempted to develop a rehabilitation device with a soft actuator that does not require special knowledge of voluntary rehabilitation at home. The target joint was the shoulder joint that often moves, such as reaching in and out. Shoulder joint rehabilitation requires soft actuation with a larger moving area that can provide passive exercises for the entire shoulder. Figure 1 illustrates the construction of human shoulder joints [27]. For shoulder joint rehabilitation, it is necessary to provide passive exercise to joints such as the glenohumeral and scapulothoracic joints, as illustrated in Figure 1 [28]. Shoulder joint rehabilitation is more effective when the scapula is moved actively. In addition, because the arms and shoulders must be lifted, it is necessary to consider the weight of the upper limbs. The weight of the human upper limb is approximately 6% of body weight [29]. The average weight for 60-year-olds in Japan is approximately 67 kg [30]. The weight of the human upper limb was approximately 4 kg. Therefore, the force required to lift the upper limbs was approximately 40 N or more.

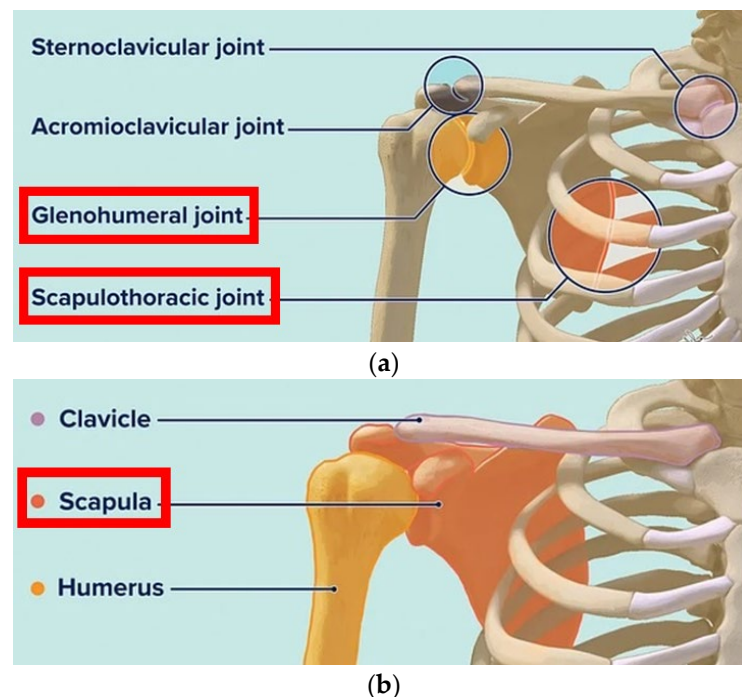


**Figure 1.** Construction of shoulder [27]. (a) Shoulder joints; (b) shoulder joint.

A rehabilitation device that users can easily release is also required because it is difficult to attach and detach wearable-type devices alone without assistance. A serious problem is that patients cannot detach immediately when they feel danger or fear. Therefore, we also attempted to develop a compact and stationary shoulder joint rehabilitation device that patients can utilize by holding their moving parts at home and nursing facilities, as demonstrated in Figure 2 [31]. It is desirable to fix the device on a table, as illustrated in

Figure 2. It is necessary to execute bending and extending motions for passive exercises, as illustrated in Figure 2b,c. As a precaution for safety, it is also necessary that hands can be easily detached from the device whenever patients feel anxious. Usually, a rehabilitation device is not utilized by one user for a long period (up to six months). It is necessary to make the device cheaply such that older adults and patients can easily buy it for voluntary home-based rehabilitation.

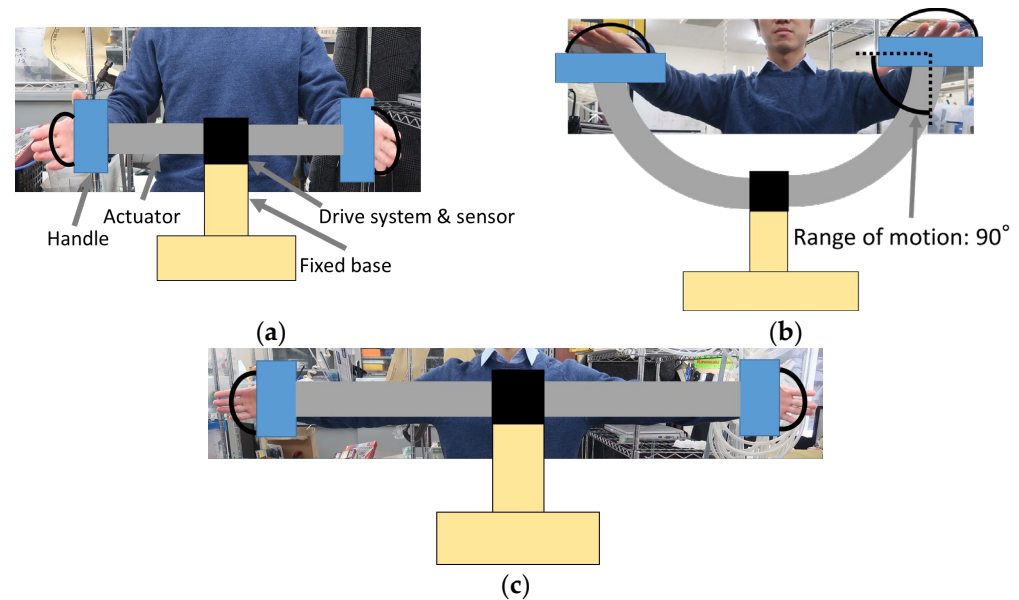


**Figure 2.** Proposal of rehabilitation device for shoulder joints. (a) Initial state; (b) bending motion; (c) extending motion.

Based on the aforementioned specifications, as a soft actuator with a larger moving area and bending stiffness that can give passive exercise, the reinforced soft actuator with a circumferential restraint utilizing some EFPAs and PET restraint plates was proposed and tested [31]. As the reinforced EFPA satisfied these specifications, a shoulder joint rehabilitation device was proposed and tested. The shoulder joints, including the scapula, were subjected to passive exercises by driving the tested device owing to the transient response. However, it is difficult for people with bedridden contracture and cerebrovascular disease to be given passive exercise because the stiffness of the actuator is insufficient. A soft actuator with a higher stiffness that can provide passive exercise, even if patients have contractures, is required.

This study proposes and tests a hexagonal pyramid-shaped EFPA (HP-EFPA) with an anisotropic stiffness with a higher stiffness in the direction of motion and a lower stiffness in other directions. Characteristics such as the bending angle, generated force, and stiffness of the HP-EFPA are described. The characteristics of the HP-EFPA were compared with those of the previous reinforced EFPA. An analytical model of the actuator was proposed for the optimal design and characteristic prediction of the HP-EFPA, and the calculated results were compared with the experimental results to confirm the validity of the proposed model.

## 2. Previous Reinforced EFPA

To develop a device with a larger driving area, an EFPA that can extend 2.5 times the initial length was proposed and tested [31]. Figure 3 illustrates the construction and motion of an EFPA. The EFPA consists of a silicone rubber tube covered with a bellows-type nylon sleeve (Swiftrans Co., Ltd., Etobicoke, ON, Canada, Stretching hose), as illustrated in Figure 3a. Both ends of the EFPA were sealed with resin. The rubber tube in the sleeve had inner and outer diameters of 8 and 11 mm, respectively, and the sleeve had inner and outer diameters of 12 and 20 mm, respectively, with a mass of 50 g. The material cost of the actuator is very low (approximately 5 US dollars per 1 m). The operating principle of the

actuator is as follows. The inner silicone rubber tube expands in radial and longitudinal directions under the supplied pressure. As the bellows sleeve can only change in the longitudinal direction without expanding in the radial direction, the actuator extends longitudinally, as demonstrated in Figure 3b. The EFPA can extend up to approximately 250% of its original length under a pressure of 500 kPa. The durability of an EFPA was approximately 30,000 times in previous continuous expansion and contraction experiments. The typical rehabilitation exercise period is approximately three to six months. Therefore, the durability of the proposed rehabilitation device utilizing the EFPAs was sufficient during the rehabilitation period.

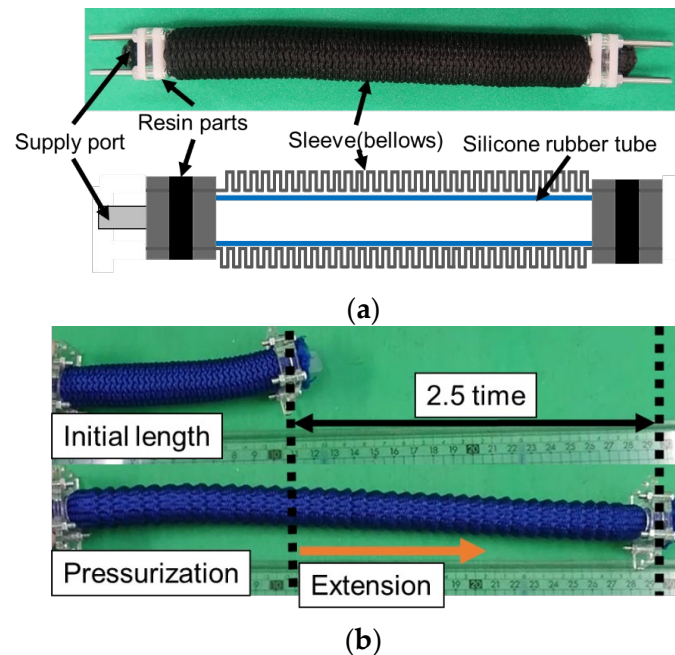


**Figure 3.** Construction and motion of EFPA. (a) View and construction of EFPA. (b) Appearance of extension motion in EFPA.

In a previous study, we developed a reinforced EFPA and applied it as a rehabilitation device for shoulder joints [31]. Figure 4 presents an overview and schematic of the previously reinforced EFPA with circumferential restraints utilizing nine EFPAs and PET restraint plates. The three EFPAs arranged in parallel were put together by small restraint plates, as shown in Figure 5a, to increase the pushing and bending forces because the single EFPA in Figure 3 has a high flexibility and small bending stiffness. In addition, to obtain a larger bending stiffness for the entire actuator, the three integrated EFPAs were also combined with Y-shaped restraint plates, as shown in Figure 5b. Via this configuration, the pushing force and bending stiffness of the reinforced EFPA became larger: the maximum pushing force was about 180 N (20 N per one EFPA), and the maximum bending stiffness and torque of the actuator were 53.1 N/(−) and 25 Nm, respectively. Adopting the reinforced EFPA, we produced a rehabilitation device for shoulder joints and attempted to control the attitude of the tested device, as demonstrated in Figure 6. In the experiment, the shoulder joints and scapula of the user were successfully subjected to passive exercise via the circular orbital motion of the tested rehabilitation device utilizing an analytical model for attitude control. However, the previous reinforced EFPA comprised nine EFPAs. Considering their utilization in homes and nursing facilities, rehabilitation devices must be lightweight and inexpensive. Therefore, it is necessary to develop another lightweight mechanism to increase the generated force and torque of the flexible actuators by decreasing the number of EFPAs.

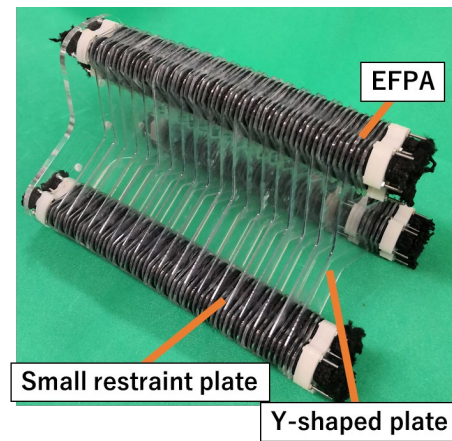


Figure 4. Overview of previous reinforced EFPA.

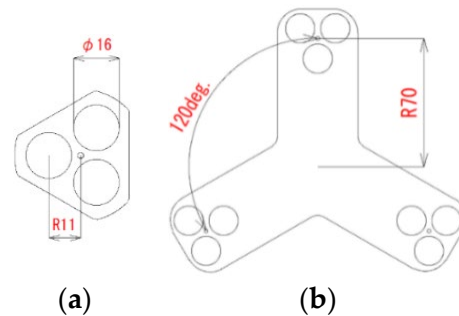


Figure 5. Shape of restraint plates (thickness of 1 mm). (a) Small restraint plate; (b) Y-shaped plate.

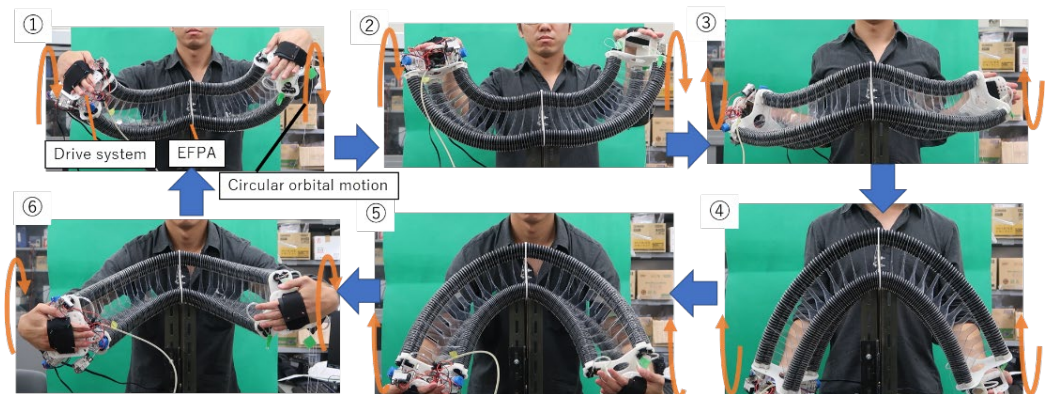
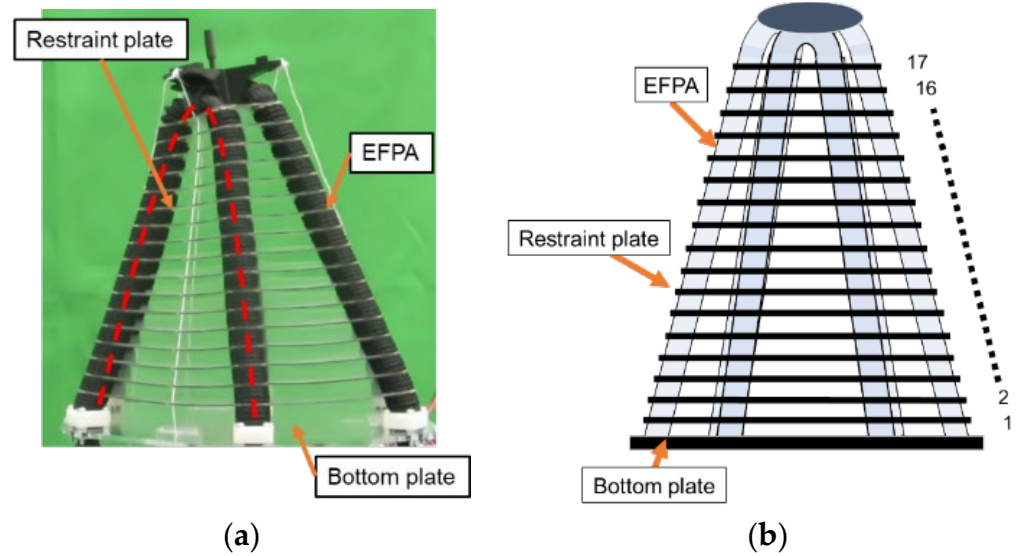


Figure 6. Appearance of passive exercise by previous device.

### 3. Hexagonal Pyramid-Shaped Actuator with Anisotropic Stiffness

#### 3.1. Construction of Hexagonal Pyramid-Shaped EFPA

To rehabilitate persons with contractures, we developed a soft actuator with a bending stiffness that generated force better than the previous actuator. The stiffness in the horizontal direction of the soft actuators, including the EFPA, was small owing to their high flexibility. Enhancing the stiffness in the horizontal direction is necessary to prevent buckling and improve safety. Therefore, a flexible actuator, restrained to a hexagonal pyramid shape to enhance the stiffness only in the direction of motion and not in the entire direction, is proposed and tested. This implies that the stiffness in the other directions of the HP-EFPA remained small. We call it “anisotropic stiffness”. Figure 7 presents an overview and schematic of the HP-EFPA with anisotropic stiffness.



**Figure 7.** Hexagonal pyramid shape of EFPA. (a) Overview; (b) schematic.

The length of the EFPAs was 400 mm. The height and mass of the HP-EFPA were 200 and 890 g, respectively. The actuator configuration is as follows. The three EFPAs bent at an angle of  $30^\circ$ , as illustrated in Figure 8a, were restrained with hexagonal restraint plates, as illustrated in Figure 9.  $i$  in the figure is the number of restraint plates, which are numbered from the bottom, as illustrated in Figure 7b. In Figure 9, the same-colored holes depict one connected EFPA arranged every  $120^\circ$ . The hole diameter in each plate was 16 mm to avoid interrupting the extension motion of the EFPA. The number of restraint plates was decided as 17 based on a previous reinforced EFPA [31], and the restraint interval of the HP-EFPA was four pitches. The radius of the bottom plate was 89 mm. The radius of each restraint plate,  $r_i$ , is decreased every 3.8 mm from the bottom plate. This indicates that each separate EFPA was inclined at an angle of  $60^\circ$ , as illustrated in Figure 8b. Thus, the actuator's stiffness can be increased by constructing a triangular truss structure, as illustrated in Figure 7. In addition, the stiffness of the HP-EFPA was further enhanced by reducing the interval restraint.

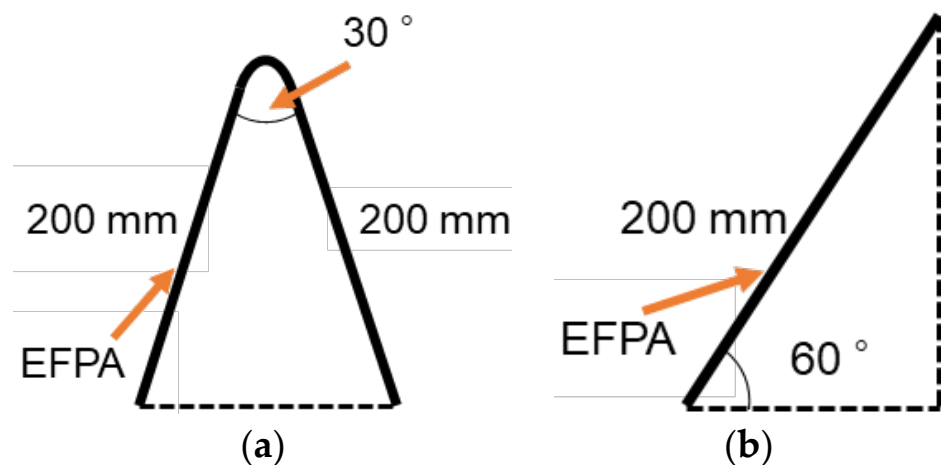


**Figure 8.** Position of each EFPA in HP-EFPA. (a) Slanted view; (b) side view.

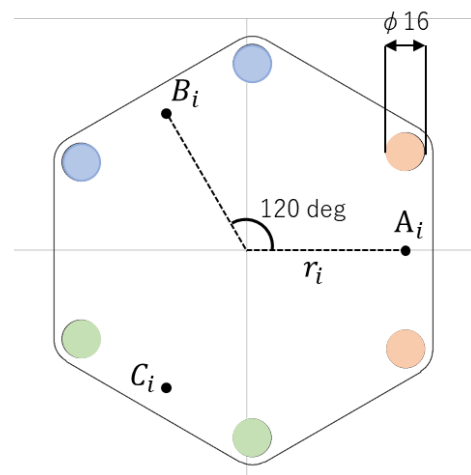


**Figure 9.** Hexagonal-shaped restraint plate.

The operating principle of the HP-EFPA is as follows. When one or two EFPAs were pressurized, the corresponding EFPAs were extended. The HP-EFPA then performed a bending motion because the other EFPAs did not extend, as demonstrated in Figure 10a. This is because the pulling force of the other EFPA was larger than the pushing force of the extended EFPAs. The HP-EFPA also extended upward by pressurizing all the EFPAs, as illustrated in Figure 10b.

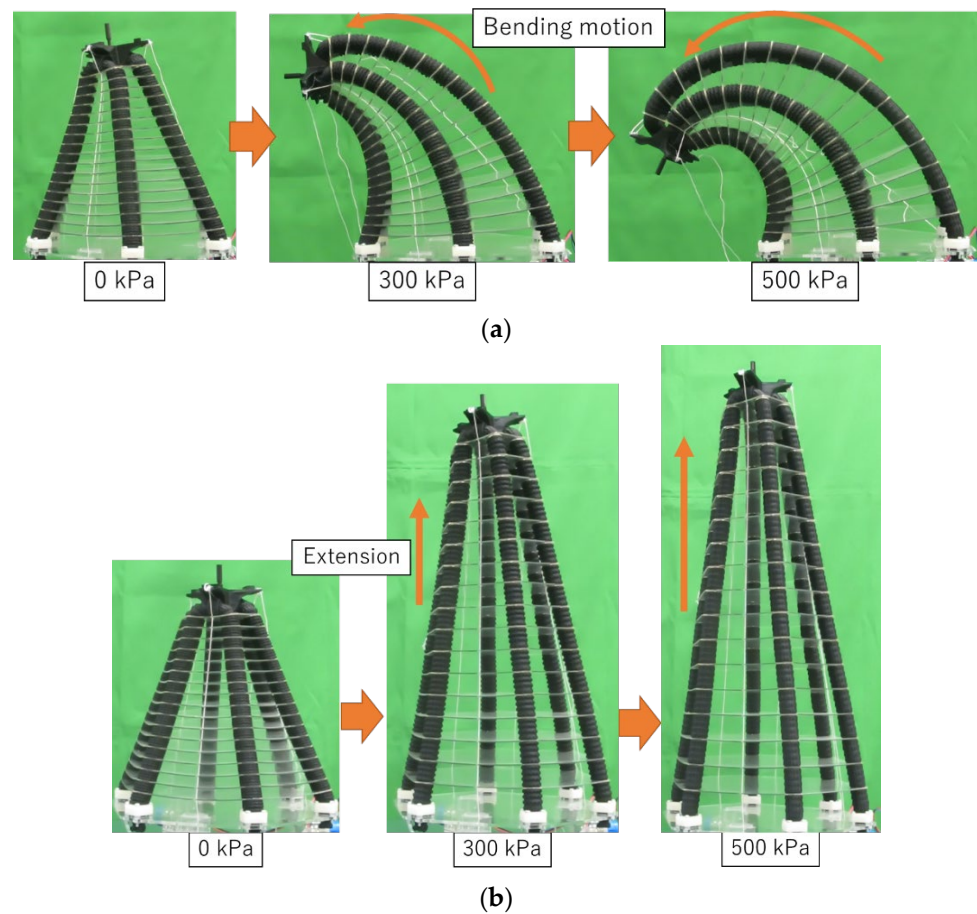


**Figure 10.** View of bending and extending motion of HP-EFPA for several pressures. (a) Pressurization of one or two EFPAs; (b) pressurization of all EFPAs.

### 3.2. Characteristic of Hexagonal Pyramid-Shaped Actuator

Figure 11 illustrates the relationship between the input pressure and the bending angle when one or two EFPAs are pressurized. In Figure 11, the circles and squares represent the experimental results when one or two EFPAs were pressurized, respectively. The solid and broken lines denote the results obtained when the input pressure was increased and decreased, respectively. In the experiment, the bending angle of the HP-EFPA was measured when it was pressurized and decompressed from 0 to 500 kPa every 50 kPa, and the experiment was repeated three times. The bending angle of the HP-EFPA could be changed by increasing the input pressure. However, a relatively large hysteresis is observed, as illustrated in Figure 11. It is considered that the frictional force between the silicone rubber tube and the bellows sleeve causes the hysteresis. The maximum bending angle of the actuator is approximately  $140^\circ$ . The required range of the bending angle for the rehabilitation of shoulder joints is more than  $90^\circ$ . Therefore, the bending angle of the proposed actuator satisfies this requirement.

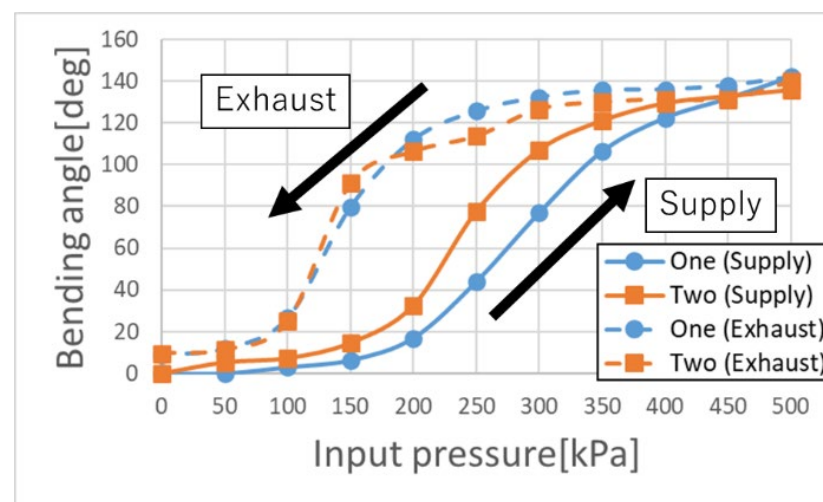


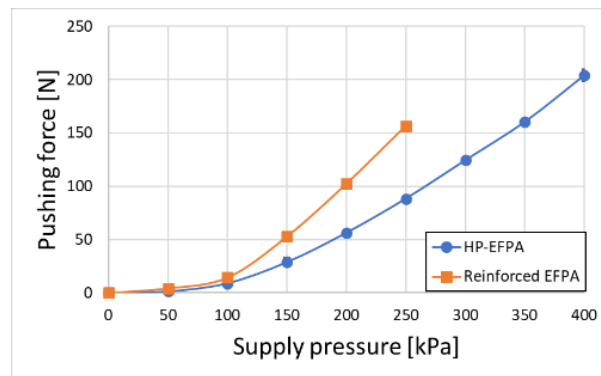
**Figure 11.** Relationship between input pressure and bending angle.

Subsequently, the generated force and stiffness of the HP-EFPA are described. Figure 12 illustrates the experimental setup adopted to measure the pushing force of the tested actuator. In the experiment, the HP-EFPA was connected in series to a force sensor (NIDEC-SHIMPO Corp., Kyoto, Japan, FGJN-50). The three EFPAs were pressurized every 50 kPa until the tested actuator buckled, and the sensor measured each pushing force. Figure 13 depicts the relationship between the supply pressure and the pushing force of the HP-EFPA. In Figure 13, the circles represent the pushing force of the tested actuator of the HP-EFPA, and the squares represent the pushing force of the previous reinforced EFPA, as illustrated in Figure 4. The tested actuator buckled when pressurized at 450 kPa. In contrast, the previous reinforced EFPA buckled at 300 kPa. Therefore, the pushing force of the reinforced EFPA could not be measured. The maximum pushing force of the tested actuator is approximately 200 N (33.3 N per EFPA). Compared with the previous reinforced EFPA, the tested HP-EFPA did not buckle, even when a supply pressure of 400 kPa was applied. Therefore, the pushing force was larger than that of the previously reinforced EFPA. This was caused by the truss structure of the HP-EFPA.

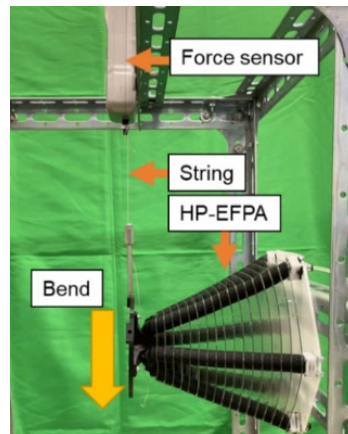
Figure 14 presents the experimental setup utilized to measure the vertical bending force of the HP-EFPA. The tested actuator was fixed to a stand in the experiment, as demonstrated in Figure 14. The HP-EFPA handle is connected to the force sensor in parallel. The input pressure was applied in steps of 50 kPa until the HP-EFPA buckled, and each vertical bending force was measured with the force sensor.



**Figure 12.** Experimental setup adopted for measuring pushing force.



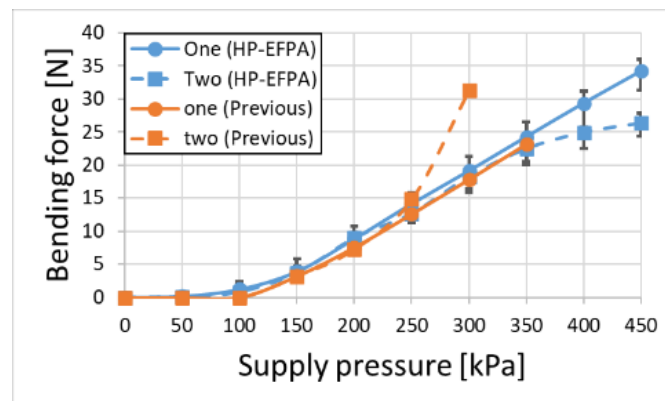
**Figure 13.** Relationship between supply pressure and pushing force.



**Figure 14.** View of experimental setup to measure vertical bending force.

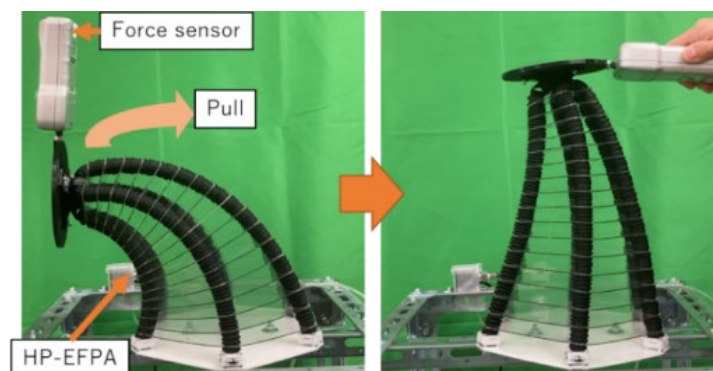
Figure 15 depicts the relationship between the supply pressure and the vertical bending force. In Figure 15, each symbol denotes the vertical bending force that occurs when the supply pressure is applied to one or two EFPA. The color represents the type of device: blue symbols depict the results of the tested HP-EFPA, and orange symbols depict those of the previous reinforced EFPA. The figure demonstrates that the bending force in the vertical direction increased linearly with an increase in the supply pressure. The maximum bending force of 35 N was larger than that of the previous reinforced EFPA. Furthermore, the pushing force of the HP-EFPA could be measured up to a supply pressure of 450 kPa without buckling. This was caused by the truss structure of the HP-EFPA. The reason for the difference between the cases of single and double pressurization at a high supply

pressure is as follows. In the case of the previous reinforced EFPA, each EFPA was parallel, as illustrated in Figure 4. The greater the number of pressurized EFPAs, the larger the bending force. This was more noticeable at higher pressures. However, in the case of the HP-EFPA, where the EFPA is unified at the apex, the influence of the EFPA that is not pressurized becomes a problem. In other words, the higher the supply pressure, the more the EFPA buckles. In the case of double pressurization with a less unpressurized EFPA, it becomes difficult to maintain the HP-EFPA shape. Therefore, at 400 kPa or higher, the pressurized EFPAs began to buckle, and the bending force became smaller than that of single pressurization.



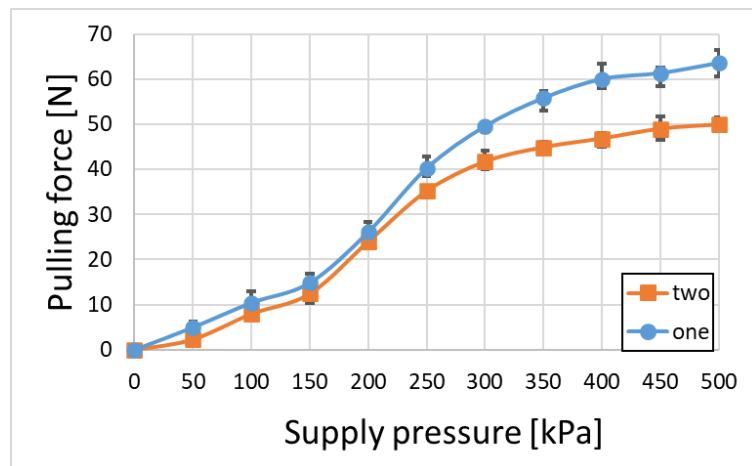
**Figure 15.** Relationship between supply pressure and bending force.

Figure 16 illustrates the measured pulling force of the HP-EFPA when it was driven during the bending motion. On the left side of Figure 16, the force sensor connected to the HP-EFPA is pulled when a bending motion drives it, and the experiment is repeated ten times.



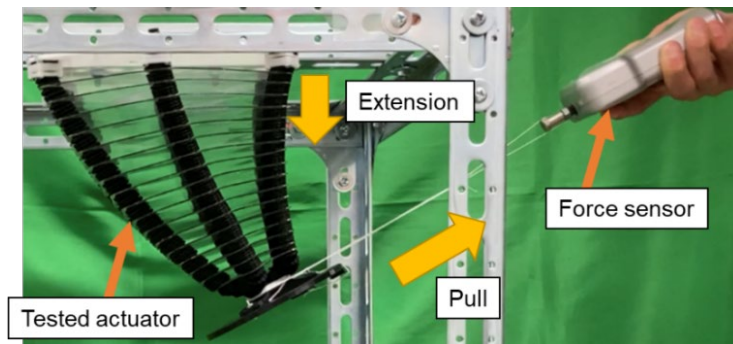
**Figure 16.** View of measurement of pulling force when HP-EFPA is driven in bending motion.

Figure 17 depicts the relationship between the supply pressure and pulling force of the bending HP-EFPA. Consequently, the maximum pulling forces applied to one or two EFPAs were approximately 63 and 50 N, respectively. As the length of the upper limb is approximately 0.7 m [32], the calculated torque becomes 35–44 Nm, and the maximum torque of 44 Nm can satisfy the target torque of 42.5 Nm. The reason why the case of the single pressurization has a larger pulling force can be considered as follows. As demonstrated in Figure 16, the unpressurized EFPA was forcibly pulled and extended when the actuator was pulled. Therefore, a larger pulling force is required because more EFPAs are not pressurized in the case of a single pressurization.



**Figure 17.** Relationship between supply pressure and pulling force.

Figure 18 illustrates the measured bending stiffness of the HP-EFPA. In the experiment, the vertical pulling force acting on the top end of the HP-EFPA and the deflection and length of the HP-EFPA were measured when extended by applying the same pressure to each EFPA. The deflection is defined as the distance between the top of the actuator and the vertical line, and the length is the EFPA length between the top and bottom plates. The deflection/length ratio was obtained from the measurement, and the ratio of the pulling force was defined as the bending stiffness.



**Figure 18.** View of measurement of bending stiffness of HP-EFPA.

Figure 19 illustrates the relationship between the deflection/length ratio and pulling force for various supply pressures. The slope of the graph represents the bending stiffness. In Figure 19, each color indicates the magnitude of the supply pressure. From the figure, the results of the start and end points on the  $x$ -axis are different because the HP-EFPA is extended according to the applied pressure, even if the deflection value is the same. It was found that the bending stiffness of the HP-EFPA fell within the range of 108–65 N/(-). Figure 20 presents the bending stiffness results of the previous reinforced EFPA with four pitches for comparison with the previous one [31]. The bending stiffness of the previous one falls within the range of 38–47 N/(-) and is about half smaller than that of the tested HP-EFPA. Therefore, the bending stiffness of the tested actuator is much improved compared with the previous one. This implies that the stiffness of the HP-EFPA was reinforced by arranging the EFPAs circumferentially and utilizing a truss structure.

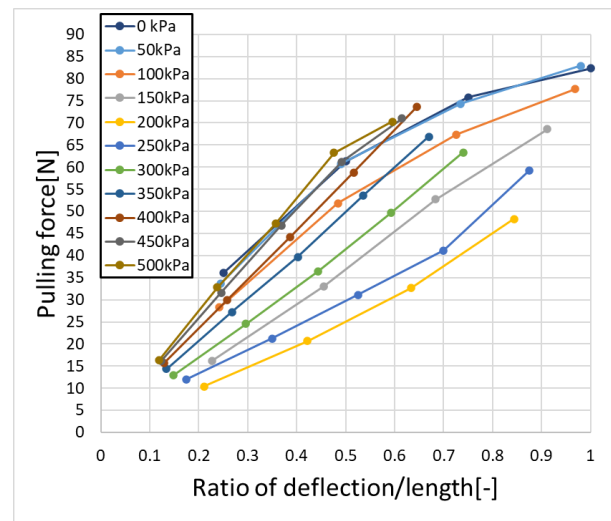


Figure 19. Relationship between ratio of deflection/length and pulling force of HP-EFPA.

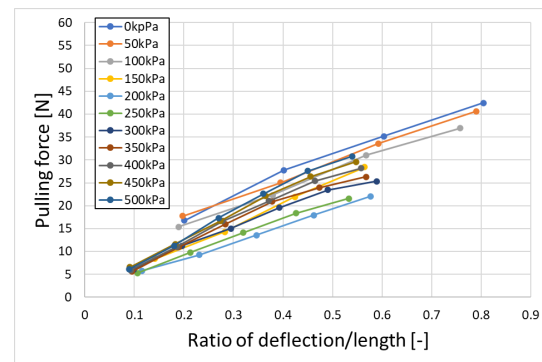


Figure 20. Relation between ratio of deflection/length and pulling force of previous one [31].

An HP-EFPA with an anisotropic restraint, which satisfies the requirement for shoulder rehabilitation, was proposed and tested. It is necessary to predict the characteristics and shape of the proposed actuator restrained by different pitches to design it. Therefore, an analytical model that can predict the characteristics and motion of the HP-EFPA is proposed in the next section.

#### 4. Analytical Model of Hexagonal Pyramid Shape of EFPA

An analytical model is proposed to predict the characteristics and motion of the proposed actuator under the supply pressure. Firstly, the virtual EFPA utilized in the analytical model is explained. Figures 21 and 22 illustrate the HP-EFPA model expressed only by the restraint plate, center lines of each EFPA, and virtual EFPA to explain the terms and variables in the proposed analytical model. Figure 21 illustrates the restraint plates and centerlines of the real EFPAs 1–3 and virtual EFPAs A–C. The virtual EFPA is between the middle position and real EFPAs, as illustrated in Figure 21. The lengths of the virtual EFPAs A–C were  $L_A$ ,  $L_B$ , and  $L_C$ , respectively. Figure 21 also presents the definitions of bending direction angle  $\alpha$  and bending angle  $\beta$ . The bending direction angle  $\alpha$  is defined as the angle counterclockwise from the  $x$ -axis. The bending angle  $\beta$  is defined as the angle from the  $z$ -axis. To calculate the shape of the tested actuator, it is necessary to know the bending direction angle  $\alpha$ , bending angle  $\beta$ , and length  $L_A$ ,  $L_B$ , and  $L_C$ . The bending angle  $\beta$  can be obtained by calculating the inclination of each restraint plate. The bending direction angle  $\alpha$  can be known by calculating the inclination direction of the restraint plate. Figure 22 presents an enlarged view of the two restraint plates in Figure 21. The radius of each restraint plate,  $r_i$ , which is the distance between the center of the restraint plate

and the virtual EFPA, was decreased every 3.8 mm from the bottom plate, as illustrated in Figure 9.

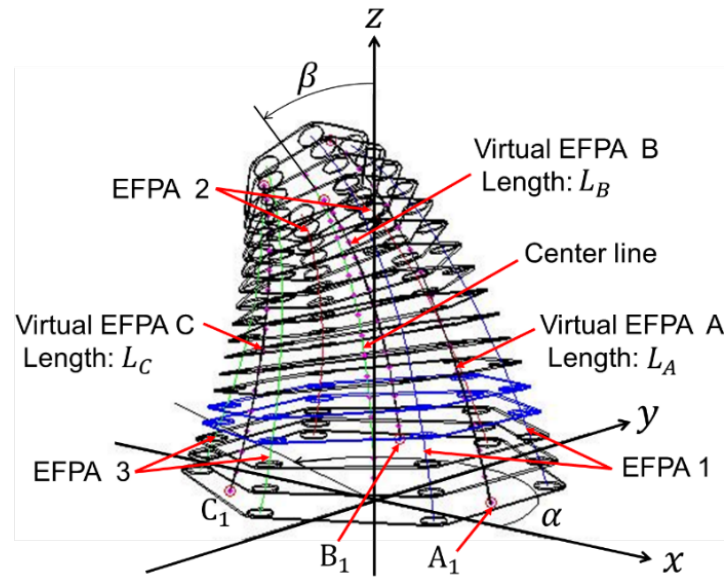


Figure 21. Restraint plates, virtual EFPA, and real EFPA of HP-EFPA.

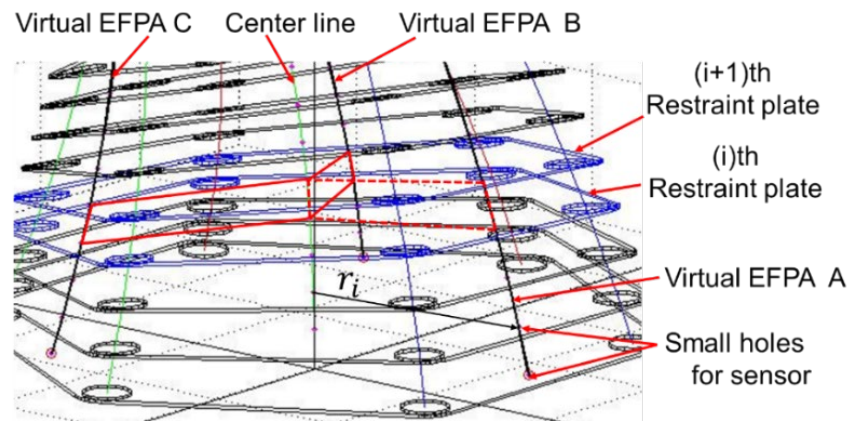


Figure 22. Enlarged view of restraint plates in Figure 21.

The coordinates of the first restraint plate in Figure 21 are represented as  $A_1(r_1, 0, h_{A1})$ ,  $B_1(-\frac{1}{2}r_1, \frac{\sqrt{3}}{2}r_1, h_{B1})$ , and  $C_1(-\frac{1}{2}r_1, -\frac{\sqrt{3}}{2}r_1, h_{C1})$  from Figure 9, respectively.  $h_{A1}$ ,  $h_{B1}$ , and  $h_{C1}$  represent the heights between the base and the first restraint plate, respectively. Figure 23a illustrates the geometry of the two restraint plates enclosed by the red broken lines in Figure 22. From the geometric relationship illustrated in Figure 23a, the height  $h_{ji}$  is given by

$$h_{ji} = (l_0 + l_j) \sin(\beta_i + \theta) \quad (j = A, B, C, i = 1, 2, \dots, m) \tag{1}$$

where  $l_0$ ,  $l_j$ ,  $\beta_i$ ,  $\theta$ , and  $m$  are the initial length of the interval plates (=8.8 mm), displacement of interval plate, bending angle of each plate, initial angle of virtual EFPA (=63.7°), and number of restraint plates ( $m = 17$ ), respectively. In the analytical model, the displacement  $l_j$  is assumed to be the same for each virtual EFPA.

Based on the characteristics of the pressure displacement of the virtual EFPA between the restraint plates measured with a displacement sensor and an EFPA, as illustrated in Figure 24, the relationship between the displacement  $l_j$  (mm) of the interval plate and supply pressure  $p_j$  (kPa) can be expressed by the following empirical formula:

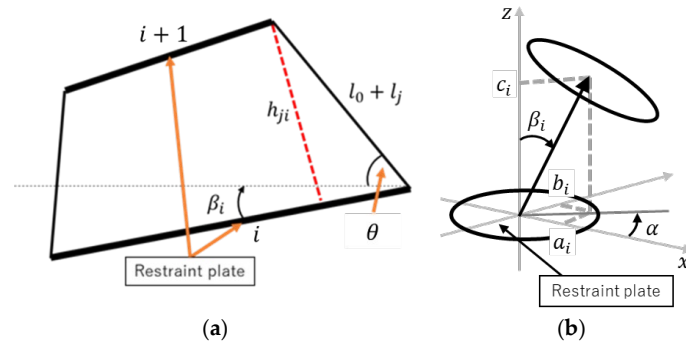


**Figure 23.** Analytical model of each interval restraint plate. (a) Geometric of height  $h_{ji}$  between plates; (b) relationship of angle  $\beta_i$  and vector  $\vec{n}_i$ .

$$l_j = -8.950 \times 10^{-10} p_j^4 + 7.240 \times 10^{-7} p_j^3 - 9.698 \times 10^{-5} p_j^2 + 4.595 \times 10^{-3} p_j + 4.934 \times 10^{-4} \quad (j = A, B, C) \quad (2)$$

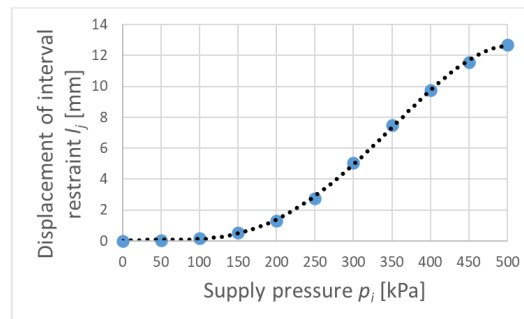


**Figure 24.** Relation between supply pressure and displacement of virtual EFPA between restraint plates.

The bending angle  $\beta_i$  of each plate becomes larger as the number  $i$  increases because the radius of the restraint plate  $r_i$  becomes smaller gradually. The radius of the restraint plate  $r_i$  can be obtained with the following equation.

$$r_{i+1} = r_i - d, \quad (3)$$

where  $b$  is the difference between each plate (3.8 mm) and  $r_1$  is 89 mm. To know the angle  $\beta_i$  of each plate, it is necessary to calculate a normal vector of  $\vec{n}_i$  as demonstrated in Figure 23b. When the normal vector is expressed  $\vec{n}_i = (a_i, b_i, c_i)$ , the following expression is obtained.

$$\vec{n}_i = \begin{bmatrix} \frac{2h_{Ai} - h_{Bi} - h_{Ci}}{r_i(h_{Ai} + h_{Bi} + h_{Ci})} d \\ \frac{3(h_{Bi} - h_{Ci})}{\sqrt{3}r_i(h_{Ai} + h_{Bi} + h_{Ci})} d \\ \frac{-3}{h_{Ai} + h_{Bi} + h_{Ci}} d \end{bmatrix} = \begin{bmatrix} \frac{h_{Bi} + h_{Ci} - 2h_{Ai}}{3r_i} \\ \frac{\sqrt{3}(h_{Ci} - h_{Bi})}{3r_i} \\ 1 \end{bmatrix} \quad (i = 1, 2, \dots, m). \quad (4)$$

The above equation means the following:

$$a_i = \frac{h_{Bi} + h_{Ci} - 2h_{Ai}}{3r_i} \quad (i = 1, 2, \dots, m); \quad (5)$$

$$b_i = \frac{\sqrt{3}(h_{Ci} - h_{Bi})}{3r_i} \quad (i = 1, 2, \dots, m). \quad (6)$$

From Equations (4) to (6) and the geometric relationship as represented in Figure 23b, the bending direction angle  $\alpha$  and bending angle  $\beta_i$  can be expressed as follows.

$$\alpha = \tan^{-1} \left( \frac{b_i}{a_i} \right), \quad (7)$$

$$\beta_i = \cos^{-1} \left( \frac{1}{\sqrt{a_i^2 + b_i^2 + 1}} \right). \quad (8)$$

As expressed in Equations (1), (5), (6), and (8), a non-linear system of equations needs to be solved to know the bending angle  $\beta_i$ . Therefore, for convenience, the following equation is utilized instead of Equation (1). This means that the lower plate angle  $\beta_{i-1}$  is utilized instead of  $\beta_i$ . Here, the bottom base angle  $\beta_0$  is assumed to be  $0^\circ$ .

$$h_{ji} = (l_0 + l_j) \sin(\beta_{i-1} + \theta) \quad (j = A, B, C, i = 1, 2, \dots, m) \quad (9)$$

The entire bending angle  $\beta$  which is the inclined angle of the top restraint plate from the base plane of the HP-EFPA can be expressed by Equation (10).

$$\beta = \sum_{i=1}^m \beta_i \quad (10)$$

Finally, the lengths of the virtual EFPAs can be obtained by Equation (11).

$$L_j = \sum_{i=1}^m (l_0 + l_j) \quad (j = A, B, C) \quad (11)$$

Based on Equations (4) to (9), the bending angle  $\beta$  of the HP-EFPA was calculated. Figure 25 compares the bending angles between the calculated and experimental results. In Figure 25, the circles and squares denote the experimental results when one or two EFPAs were pressurized, respectively, and the solid line indicates the calculated results. The results indicated that the calculated bending angle of the tested actuator for one EFPA generally agreed with the experimental results. However, differences were observed between the calculated and experimental results when the two EFPAs were pressurized. The reasons for this are as follows. Compared with one pressurized EFPA, two pressurized EFPAs can extend more because they affect one EFPA. In the analytical model, such interference between the EFPAs was not considered, which will be our future study's focus.

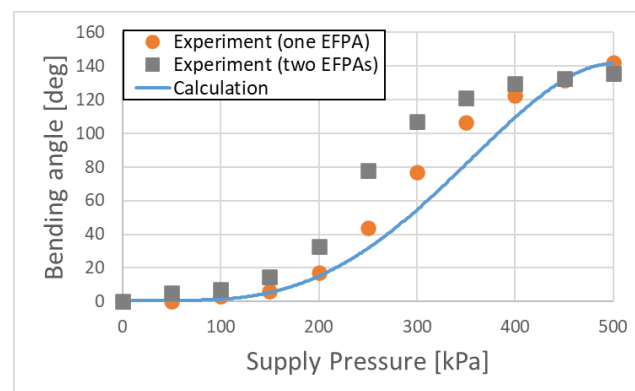


**Figure 25.** Comparison of bending angle between calculation and experiment.

The length of virtual EFPA A was calculated with Equation (11). Figure 26 compares the lengths from the calculated and experimental results. In Figure 26, the solid lines and squares denote the calculated and experimental results, respectively, when EFPA 1 was pressurized. In the experiment, the length of virtual EFPA A was measured with a developed wire-type linear potentiometer [33] and small holes for the virtual EFPA in the restraint plate, as illustrated in Figure 22. According to Figure 26, the calculated lengths agree well with the experimental results.

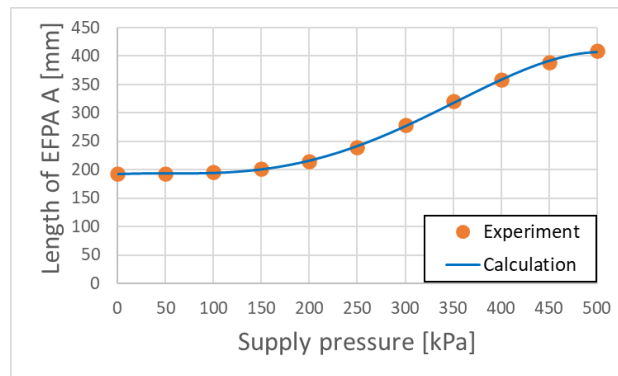


Figure 26. Comparison of length of virtual EFPA A between calculation and experiment.

Finally, Figure 27a,b illustrate the postures of the HP-EFPA simulated with MATLAB and the experimental postures during the operation of the tested actuator, respectively. These are the calculated postures of the tested actuator when the bending angle  $\beta$  is kept at  $90^\circ$  and the bending direction angle  $\alpha$  is changed every  $60^\circ$ . Figure 27 implies that the operation of the HP-EFPA can be simulated well with the proposed analytical model. Thus, it was confirmed that the proposed analytical model of the HP-EFPA is valid. A future study will develop a shoulder rehabilitation device utilizing a tested actuator, displacement sensor, embedded controller, and servo valves to control the EFPA. The developed rehabilitation device will be evaluated with PTs. In addition, the pressure-displacement characteristics of the HP-EFPA expressed in Equation (2) should be modeled theoretically.

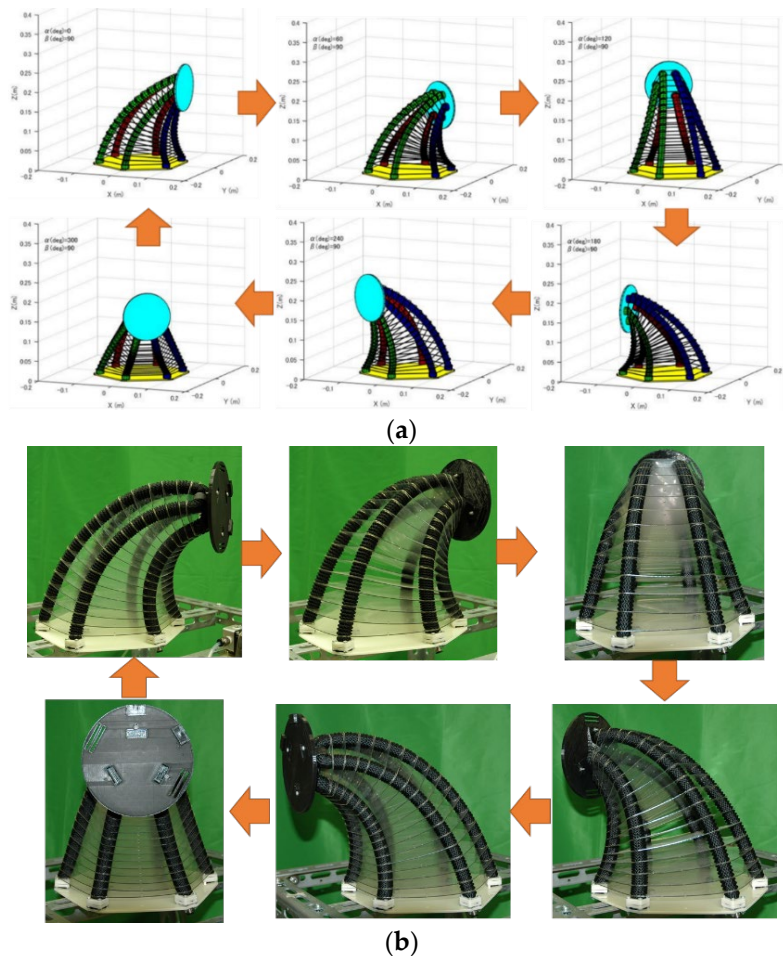


Figure 27. Construction and motion of EFPA. (a) Simulated postures; (b) experimental postures.

## 5. Conclusions

This study attempted to develop an HP-EFPA for a shoulder rehabilitation device and propose an analytical model for predicting its characteristics and motion, summarized as follows. As a flexible actuator of a rehabilitation device that can provide passive exercise to patients with contractures, an HP-EFPA with anisotropic stiffness, which has a high stiffness in the direction of motion and flexibility in other directions utilizing a truss structure, and the elastic force of the rubber tube was proposed and tested. The restraint method and operating principles were also described. The characteristics of the HP-EFPA, such as the bending angle, generated force, and bending stiffness, were measured. The results confirmed that the HP-EFPA satisfied the assumed specification. The stiffness of the proposed actuator was improved by approximately twice that of the previous reinforced EFPA, even when the number of EFPAs was reduced. An analytical model of the actuator is proposed to predict the characteristics of the proposed HP-EFPA. The calculated bending angles generally agree with the experimental angles at various supply pressures. Furthermore, the bending posture of the HP-EFPA was calculated with MATLAB, and the movement of the actuator was simulated.

**Author Contributions:** Conceptualization, S.S., H.H. and A.G.; methodology, S.S., H.H. and A.G.; validation, S.S. and H.H.; Formal analysis, S.S., H.H. and A.G.; investigation, S.S., H.H. and A.G.; data curation, S.S. and H.H.; writing—original draft preparation, S.S.; writing—review and editing, S.S.; funding acquisition, S.S. All authors have read and agreed to the published version of the manuscript.

**Funding:** This work was supported by the Fluid Power Technology Promotion Foundation of Japan (Grant Number 202005).

**Data Availability Statement:** Data are contained within the article.

**Conflicts of Interest:** The authors declare no conflict of interest.

## References

1. Statistics Bureau of Japan Ageing Society. Available online: <https://www.stat.go.jp/data/topics/topi1321.html/> (accessed on 28 December 2022).
2. Council of Bureau of Social Welfare and Public Health Tokyo Metropolitan Government. Available online: [https://www.fukushihoken.metro.tokyo.lg.jp/iryo/sonota/riha\\_iryu/kyougi01/rehabiri24.files/siryu242.pdf](https://www.fukushihoken.metro.tokyo.lg.jp/iryo/sonota/riha_iryu/kyougi01/rehabiri24.files/siryu242.pdf) (accessed on 20 February 2023).
3. Zimmermann, Y.; Forino, A.; Riener, R.; Hutter, M. A Versatile and Dynamic Upper-Limb Rehabilitation Robot. *IEEE Robot. Autom. Lett.* **2019**, *4*, 3649–3656. [[CrossRef](#)]
4. Tang, L.; Liu, G.; Yang, M.; Li, F.; Ye, F.; Li, C. Joint design and torque feedback experiment of rehabilitation robot. *Adv. Mech. Eng.* **2020**, *12*, 1687814020924498. [[CrossRef](#)]
5. Zhang, L.; Guo, S.; Sun, Q. Development and Assist-As-Needed Control of an End-Effector Upper Limb Rehabilitation Robot. *Appl. Sci.* **2020**, *10*, 6684. [[CrossRef](#)]
6. Dong, M.; Fan, W.; Li, J.; Zhou, X.; Rong, X.; Kong, Y.; Zhou, Y. A New Ankle Robotic System Enabling Whole-Stage Compliance Rehabilitation Training. *IEEE/ASME Trans. Mechatron.* **2021**, *26*, 1490–1500. [[CrossRef](#)]
7. Yokota, M.; Takaiwa, M. Gait Rehabilitation System Using a Non-Wearing Type Pneumatic Power Assist Device. *J. Robot. Mechatron.* **2021**, *33*, 927–934. [[CrossRef](#)]
8. Feng, G.; Zhang, J.; Zuo, G.; Li, M.; Jiang, D.; Yang, L. Dual-Modal Hybrid Control for an Upper-Limb Rehabilitation Robot. *Machines* **2022**, *10*, 324. [[CrossRef](#)]
9. Mandeljc, A.; Rajhard, A.; Muni, M.; Kamnik, R. Robotic Device for Out-of-Clinic Post-Stroke Hand Rehabilitation. *Appl. Sci.* **2022**, *12*, 1092. [[CrossRef](#)]
10. Li, Y.; Gong, Y.; Zhuang, J.; Yang, J.; Osawa, K.; Nakagawa, K.; Lee, H.; Yuge, L.; Tanaka, E. Development of Automatic Controlled Walking Assistive Device Based on Fatigue and Emotion Detection. *J. Robot. Mechatron.* **2022**, *34*, 1383–1397. [[CrossRef](#)]
11. Nguyen, T.; Bui, T.; Pham, H. Using proposed optimization algorithm for solving inverse kinematics of human upper limb applying in rehabilitation robotic. *Artif. Intell. Rev.* **2022**, *55*, 679–705. [[CrossRef](#)]
12. Sasaki, D.; Noritsugu, T.; Yamamoto, T.; Takaiwa, M. Development of Power Assist Glove using Pneumatic Artificial Rubber Muscle. *J. Robot. Mechatron.* **2006**, *24*, 640–646.
13. Noritsugu, T.; Takaiwa, M.; Sasaki, D. Development of Power Assist Wear Using Pneumatic Rubber Artificial Muscles. *J. Robot. Mechatron.* **2009**, *21*, 607–613. [[CrossRef](#)]
14. Kawasaki, H.; Ito, S.; Ishigure, Y.; Nishimoto, Y.; Aoki, T.; Abe, M.; Sakaeda, H.; Ojika, T.; Mouri, T.; Ueki, S. Hand Rehabilitation Assist Robot Designed with Assistance for Thumb Opposability. *Trans. Jp. Soc. Mech. Eng.* **2008**, *74*, 3019–3027. [[CrossRef](#)]

15. Taniguchi, H.; Wakimoto, S.; Suzumori, K. Development of a hand rehabilitation system to prevent contracture for finger joints based on the therapy of occupational therapists. *Trans. Jp. Soc. Mech. Eng.* **2014**, *80*, TRANS0348.
16. Polygerinos, P.; Wang, Z.; Galloway, K.; Wood, R.; Walsh, C. Soft robotic glove for combined assistance and at-home rehabilitation. *Robo. Auto. Sys.* **2015**, *73*, 135–143. [[CrossRef](#)]
17. Aliff, M.; Dohta, S.; Akagi, T. Simple Trajectory Control Method of Robot Arm Using Flexible Pneumatic Cylinders. *J. Robot. Mechatron.* **2015**, *27*, 698–705. [[CrossRef](#)]
18. Abe, T.; Koizumi, S.; Nabae, H.; Endo, G.; Suzumori, K.; Sato, N.; Adachi, M.; Takamizawa, F. Fabrication of “18 Weave” Muscles and Their Application to Soft Power Support Suit for Upper Limbs Using Thin McKibben Muscle. *IEEE Robot. Auto. Lett.* **2019**, *4*, 2532–2538. [[CrossRef](#)]
19. Takada, M.; Wakimoto, S.; Oshikawa, T.; Ueda, T.; Kanda, T. Active Cloth Fabricated by a Flat String Machine and its Application to a Safe Wheelchair System. *J. Robot. Mechatron.* **2020**, *32*, 1010–1018. [[CrossRef](#)]
20. Nguyen, P.; Zhang, W. Design and Computational Modeling of Fabric Soft Pneumatic Actuators for Wearable Assistive Devices. *Sci. Rep.* **2020**, *10*, 9638. [[CrossRef](#)]
21. Thalman, C.; Hertzell, T.; Lee, H. Toward A Soft Robotic Ankle-Foot Orthosis (SR-AFO) Exosuit for Human Locomotion: Preliminary Results in Late Stance Plantarflexion Assistance. In Proceedings of the 2020 3rd IEEE International Conference on Soft Robotics, New Haven, CT, USA, 15 May–15 July 2020; p. 19763790.
22. Yuan, P.; Kawano, G.; Tsukagoshi, H. Design and Modeling of Soft Pneumatic Helical Actuator with High Contraction Ratio. *J. Robo. Mechatron.* **2020**, *32*, 1061–1070. [[CrossRef](#)]
23. Kimura, S.; Suzuki, R.; Machida, K.; Kashima, M.; Okui, M.; Nishihama, R.; Nakamura, T. Development of an Exoskeleton-Type Assist Suit Utilizing Variable Stiffness Control Devices Based on Human Joint Characteristics. *Actuators* **2021**, *10*, 17. [[CrossRef](#)]
24. Miyazaki, T.; Kawase, T.; Kanno, T.; Sogabe, M.; Nakajima, Y.; Kawashima, K. Running Motion Assistance Using a Soft Gait-Assistive Suit and Its Experimental Validation. *IEEE Access* **2021**, *9*, 94700–94713. [[CrossRef](#)]
25. Hoang, T.T.; Sy, L.; Bussu, M.; Thai, T.M.; Low, H.; Phan, T.P.; Davies, J.; Nguyen, C.C.; Lovell, H.N.; Do, N.T. A Wearable Soft Fabric Sleeve for Upper Limb Augmentation. *Sensors* **2021**, *21*, 7638. [[CrossRef](#)]
26. Pan, M.; Yuan, C.; Liang, X.; Dong, T.; Liu, T.; Zhang, J.; Zou, J.; Yang, H.; Bowen, C. Soft Actuators and Robotic Devices for Rehabilitation and Assistance. *Adv. Int. Sys.* **2021**, *4*, 2100140. [[CrossRef](#)]
27. SPORTS-Health “Guide to Shoulder Anatomy”. Available online: <https://www.sports-health.com/sports-injuries/shoulder-injuries/guide-shoulder-anatomy> (accessed on 28 January 2023).
28. Senda, M.; Katayama, Y.; Kaneda, D. Rehabilitation in the Shoulder Disease. *Jp. J. Reha. Med.* **2016**, *53*, 928–933. [[CrossRef](#)]
29. Ogawa, K. *Evidence-Based Nursing Ergonomics and Body-Mechanics*; Tokyo Denki University Press: Tokyo, Japan, 2008; p. 28.
30. National Institute of Health and Nutrition. Physical Condition Survey. Available online: [https://www.nibiohn.go.jp/eiken/kenkounippon21/eiyouchousa/keinen\\_henka\\_shintai.html](https://www.nibiohn.go.jp/eiken/kenkounippon21/eiyouchousa/keinen_henka_shintai.html) (accessed on 28 January 2023).
31. Shimooka, S.; Akagi, T.; Dohta, S.; Shinohara, T.; Alif, M. Development of Reinforced Extension Type Flexible Pneumatic Actuator with Circumferential Restraints and Its Application for Rehabilitation Device. *Int. J. Automot. Mech. Eng.* **2020**, *17*, 931–938. [[CrossRef](#)]
32. Artificial Intelligence Research Center (AIST). Database of Human Body Dimensions. Available online: <https://www.airc.aist.go.jp/dhrt/91-92/data/list.html> (accessed on 28 January 2023).
33. Matsui, Y.; Akagi, T.; Dohta, S.; Kobayashi, W.; Tamaki, H. Development of Flexible Spherical Actuator with 3D Coordinate Measuring Device. *J. Flow. Control Meas. Vis.* **2018**, *6*, 95–106. [[CrossRef](#)]

**Disclaimer/Publisher’s Note:** The statements, opinions and data contained in all publications are solely those of the individual author(s) and contributor(s) and not of MDPI and/or the editor(s). MDPI and/or the editor(s) disclaim responsibility for any injury to people or property resulting from any ideas, methods, instructions or products referred to in the content.